This is a repository copy of *Population inversion in optically pumped asymmetric quantum well terahertz lasers* .

White Rose Research Online URL for this paper:
http://eprints.whiterose.ac.uk/1676/

Population inversion in optically pumped asymmetric quantum well terahertz lasers

P. Harrison[a)] and R. W. Kelsall

Department of Electronic and Electrical Engineering, University of Leeds, Leeds LS2 9JT, United Kingdom

Intersubband carrier lifetimes and population ratios are calculated for three- and four-level optically pumped terahertz laser structures. Laser operation is based on intersubband transitions between the conduction band states of asymmetric GaAs-Ga$_{1-x}$Al$_x$As quantum wells. It is shown that the carrier lifetimes in three-level systems fulfill the necessary conditions for stimulated emission only at temperatures below 200 K. The addition of a fourth level, however, enables fast depopulation of the lower laser level by resonant longitudinal optical phonon emission and thus offers potential for room temperature laser operation. © *1997 American Institute of Physics.* [S0021-8979(97)04511-8]

I. INTRODUCTION

Continuing with the recent success of quantum cascade or intersubband lasers operating in the midinfrared,[1] this work is concerned with extending the emission wavelength into the farinfrared (30–300 μm) or terahertz (1–10 THz) region of the spectrum. There are many applications that could benefit from the smaller antenna size and greater possible bandwidth, including mobile telephony, high resolution radar and wireless local area network (LAN).

Terahertz emitters based on GaAs technology require a subband spacing which (for frequencies of less than 8.7 THz) is smaller than the longitudinal optical (LO) phonon energy. It was therefore thought that there is a considerable advantage in working in this frequency range since LO phonon emission—which represents the competing non-radiative loss mechanism—should be eliminated. However, recent experimental work on wide quantum wells has yielded a range of intersubband lifetimes, from 200 ps (characteristic of the acoustic phonon scattering regime)[2] to approximately 1 ps (implying incomplete suppression of LO phonon scattering).[3] Determination of intersubband lifetimes is therefore an important aspect in the successful design of both a terahertz emitter and a laser.

The two principal design parameters for a semiconductor laser are population inversion and quantum efficiency. For intersubband lasers, the quantum efficiency for a single active region is generally very low and, in the quantum cascade devices, is magnified by growing a multiple stack of active regions. Some control of the quantum efficiency can be achieved by layer design to optimise the intersubband optical matrix element, but any advantages thus obtained are likely to be dominated by the strong decrease in this matrix element with decreasing frequency.[4] However the attainment of population inversion, which is dependent on the relative repopulation and de-population rates of the participant states, is more amenable to optimisation by adjustments in layer thicknesses and material compositions; this is the focus of the theoretical work described below.

The devices considered in this article are designed for optically pumped terahertz emission using a 10.6 μm CO$_2$

pump source. Intersubband optical pumping was recently demonstrated by Julien and co-workers.[5,6] Although less convenient than electrical injection (particularly for commercial applications), optical pumping allows great simplifications in device design and fabrication compared to the quantum cascade lasers. We begin by studying a range of prototype three-level asymmetric quantum well structures:[7] an asymmetric potential is required to break the parity of the $|1\rangle$ and $|3\rangle$ states and hence permit the $|1\rangle \rightarrow |3\rangle$ pump transition. Subsequently we present calculations for four-level systems which can be designed for enhanced population inversion.

II. THEORY

The energy levels in both three- and four-level asymmetric quantum well devices were obtained by numerical solution of the effective mass Schrödinger equation.[8] The numerical wave functions were then used to calculate non-radiative (phonon scattering) transition probabilities via acoustic (deformation potential) and polar LO phonon modes. The standard Fermi's golden rule formulation was used in both cases.[9] Since we wished to investigate population inversion over a wide range of temperatures, the acoustic scattering rates were calculated without use of the usual high temperature (equipartition) or low temperature (zero point) approximations.[10] However, to reduce the CPU time, a fixed acoustic phonon energy (1 meV) was assumed when determining the allowed final states in the calculations. The LO phonon energy was also assumed to have a constant value of 36 meV.

Bulk-like phonon modes were assumed for both acoustic and LO phonon scattering. While it is clear that the phonon modes will be modified by the presence of semiconductor heterojunctions, there is much controversy over the correct theoretical description of the quantum well modes.[11,12] Recent analysis by Ridley and co-workers[13,14] appears to reconcile earlier, conflicting theories; nonetheless, our opinion is that bulk modes represent the safest starting point for obtaining approximate results, with the fine detail supplied by quantum well modes deferred to subsequent work.

The overall non-radiative intersubband lifetimes were obtained by weighting the energy dependent scattering prob-

---

[a)]Electronic mail: p.harrison@elec-eng.leeds.ac.uk

abilities ($P^{AC}(E)$ and $P^{LO}(E)$) according to the distribution functions in the initial and final subbands:

$$\frac{1}{\tau_{if}^{AC,LO}} = \frac{\int_{E_{min}}^{E_{max}} P^{AC,LO}(E)\mathscr{F}^i(E)[1-\mathscr{F}^f(E-E_{AC,LO})]dE}{\int_{E_{min}}^{E_{max}}\mathscr{F}^i(E)dE},$$

(1)

where E is the initial energy of the electron, $\mathscr{F}(E)$ is the distribution function in the initial (i) or final (f) subband and $E_{AC,LO}$ is the energy of the acoustic or LO phonons, respectively. The integrals are performed over the full range of initial state subband energies, i.e. from the subband minima ($\mathbf{k}=0$) to the top of the well.

The exact distribution functions can only be obtained by numerical or stochastic (Monte Carlo) solution of the Boltzmann transport equation, which is beyond the scope of this article. Instead, we make the common assumption that the distribution functions are thermalised by electron-electron (e-e) scattering yielding, in each subband, a Fermi-Dirac distribution function characterised by some electron temperature T_e. Since the intrasubband (e-e) scattering lifetime is of the order of 10 fs (Ref. 15), i.e., nearly two orders of magnitude faster than LO phonon scattering, this assumption is reasonable. More debatable is the role of intersubband (e-e) scattering, which re-distributes both energy and electron population between different subbands. The intersubband e-e lifetimes are longer; values across the subpicosecond-picosecond range have been calculated for the range of possible two-particle intersubband processes.[16]

The lifetimes for intersubband radiative transitions of energy $\hbar\omega$ between an initial state $|i\rangle$ and a final state $|f\rangle$ are calculated using the expression[17]

$$\frac{1}{\tau_{if}^{rad}} = \frac{ne^2\omega^2}{6\pi\epsilon_0 m^* c^3}f_{if},$$

(2)

where the oscillator strength f_{if} is given by[18]

$$f_{if} = \frac{2\hbar}{m^*\omega}\left|\left\langle i\left|\frac{\partial}{\partial z}\right|f\right\rangle\right|^2,$$

(3)

and the refractive index at terahertz frequencies was deduced by extrapolating the Sellmeier equation[19] with the 103 K fit of Seraphin and Bennett.[20]

III. RESULTS AND DISCUSSION

A. Three-level system

The three-level system was based on the single step asymmetric quantum well proposed by Berger,[17] as shown in Fig. 1. The structures are comprised of a 65 Å GaAs deep well layer with an adjacent GaAs-Ga$_{1-x}$Al$_x$As step, surrounded by Ga$_{0.76}$Al$_{0.24}$As barriers. In this system, optical pumping promotes carriers from subbands 1 to 3, while the E_3-E_2 energy separation is tuned for terahertz emission. The height x_b and width b of the step were adjusted, as displayed in Table I, in order to vary the emission wavelength while retaining the 117 meV (10.6 μm) separation of subbands $|1\rangle$ and $|3\rangle$ for CO$_2$ laser pumping. Examination of Table I shows that it is possible to tune the emission frequency across the whole range of terahertz (1–10 THz) fre-
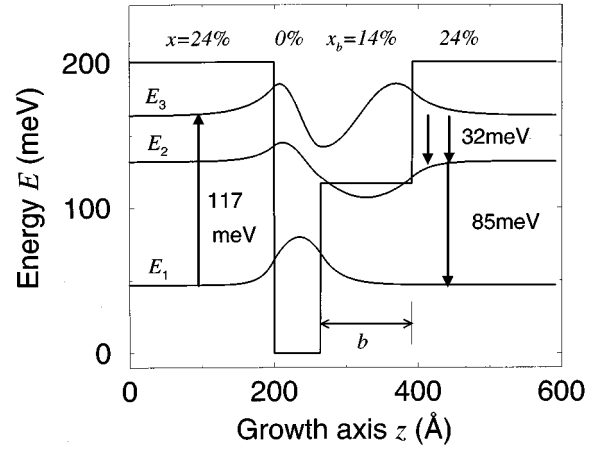

FIG. 1. Schematic diagram of the energy levels and wave functions of a three-level asymmetric quantum well. E_3-E_1 is tuned for CO$_2$ pumping, and terahertz emission is sought from $|3\rangle \rightarrow |2\rangle$ transitions (7.7 THz for this example).

quencies in a three-level CO$_2$ pumped device. However, in order to examine the potential of this three-level system as a terahertz laser, as opposed to a spontaneous emission device, it is necessary to look at the carrier dynamics that govern population inversion.

Using a simple rate equation analysis, the population n_2 of the second subband at time t is given by

$$\frac{dn_2}{dt} = \frac{n_3}{\tau_{32}} + \frac{n_3}{\tau_{32}^{rad}} - \frac{n_2}{\tau_{21}},$$

(4)

where τ_{32}^{rad} is the radiative lifetime for transitions between subbands 3 and 2, and τ_{32} and τ_{21} are the non-radiative (phonon limited) lifetimes for $|3\rangle \rightarrow |2\rangle$ and $|2\rangle \rightarrow |1\rangle$ transitions, respectively, including both acoustic and LO modes.

In the steady state $dn_2/dt=0$, and noting that $\tau_{32}^{rad} \gg \tau_{32}$ (as confirmed by the calculated radiative lifetimes at 77 K shown in Table I), then the standard *necessary* condition for population inversion ($n_3 > n_2$) is as follows:

$$\frac{1}{\tau_{21}} > \frac{1}{\tau_{32}}.$$

(5)

The ratio τ_{32}/τ_{21} then gives the predicted population inversion ratio in a device.

TABLE I. Structural parameters of the three-level asymmetric quantum well with a terahertz E_3-E_2 intersubband separation.

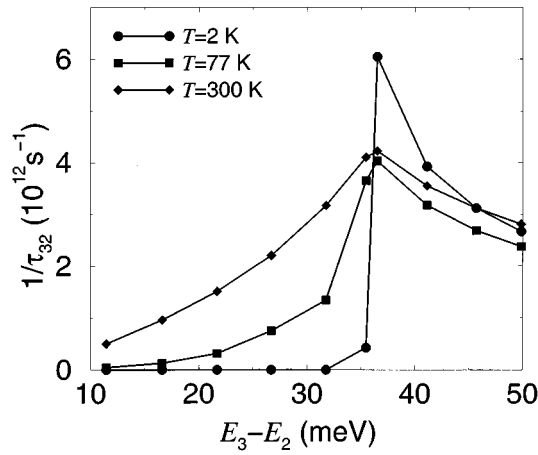| Step x_b (%)	Step width b (Å)	E_3-E_1 (meV)	E_3-E_2 (meV)	E_3-E_2 (THz)	τ_{32}^{rad} (μs)
10	101	116.988	49.851	12.1	0.35
11	105	117.321	45.708	11.1	0.43
12	111	117.117	41.119	9.9	0.54
13	118	117.154	36.504	8.8	0.70
14	127	117.179	31.750	7.7	0.95
15	140	116.899	26.695	6.5	1.37
16	157	116.902	21.684	5.2	2.13
17	182	116.992	16.612	4.0	3.74
18	224	117.143	11.454	2.8	8.14

P. Harrison and R. W. Kelsall

FIG. 2. $|3\rangle \rightarrow |2\rangle$ non-radiative (phonon scattering) rates for a range of three-level asymmetric quantum wells, defined by the $E_3 - E_2$ separations listed in Table I.

FIG. 4. Ratio of the non-radiative lifetime in the upper laser level to that in the lower level for the three-level systems.

The non-radiative lifetimes τ_{32} and τ_{21} at three different lattice temperatures are plotted in Fig. 2 and Fig. 3, respectively, for the set of structures defined in Table I and identified by the $E_3 - E_2$ energy separation. In calculating the weighted lifetimes via equation (1) the populations, $n_1 = 10^{12}$, $n_2 = 10^{10}$ and $n_3 = 10^{10}$ cm^{-2}, were assumed. These values are typical, assuming a pump power of 100 mW,[17] and the resulting scattering rates are not sensitive to small changes in them. Also, in calculating the distribution functions the electron temperature was assumed to be equal to the lattice temperature in each case. Accurate determination of the electron temperature (assuming that the distribution can be characterised by such) would require a complete solution of the Boltzmann equation.

In Fig. 2, the influence of the distribution function in subband 3 on the scattering rates can be clearly seen. At 2 K most of the n_3 population occupies states near the bottom of the subband, such that the phonon scattering rate falls off rapidly when the subband separation becomes less than the LO phonon energy. The acoustic scattering rates in all cases
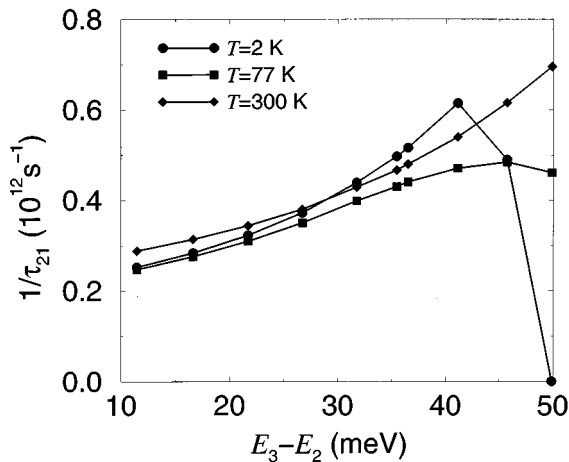

FIG. 3. $|2\rangle \rightarrow |1\rangle$ non-radiative (phonon scattering) rates for the same three-level asymmetric quantum wells as in Fig. 2. Note that the rates are plotted against $E_3 - E_2$ to enable direct comparison with Fig. 2.
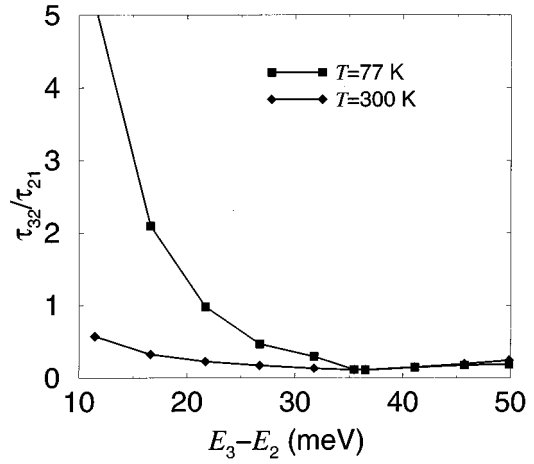
are of the order of 10^{10} s^{-1}, and are thus negligible on the scale of the graphs. As the lattice temperature is increased the energy distribution in subband 3 becomes much broader; this means that there is a substantial number of "warm" carriers (i.e., those lying well above the subband edge) that can scatter into the second subband by LO phonon emission, even when the subband separation is less the E_{LO}. Thus the scattering rate in the range $E_3 - E_2 < E_{LO}$ rises significantly with lattice temperature, and attains values well above the acoustic phonon rate. A similar effect occurs when the electron temperature is raised while maintaining a fixed lattice temperature, see Lee et al.[21] It is clear that reduction of the subband separation below E_{LO} does *not* eliminate LO phonon scattering unless both the lattice and electron temperatures are very low. This observation concurs with several experimental reports in which the measured intersubband lifetimes (for subband separations less than E_{LO}) were found to be much faster than the acoustic phonon limited values.[3,22] In practice, the measured values are sensitive to the exact experimental conditions (pump source, mode, intensity, continuous wave or pulsed operation) as well as the operating temperatures and sample specification.

In Fig. 3 the dominant effect of temperature on the $|2\rangle \rightarrow |1\rangle$ rate occurs via the energy distribution of *final* states in subband 1. At low lattice temperatures the distribution function is step-like, with almost all states below the quasi-Fermi level occupied. Thus, as the $E_2 - E_1$ separation is reduced (which corresponds to increasing the $E_3 - E_2$ separation on Fig. 3), a threshold is reached beyond which LO phonon scattering is almost completely suppressed due to Pauli exclusion. Conversely, at high temperatures thermal broadening of the subband 1 energy distribution guarantees that there are always vacant states available.

Figure 4 shows the ratio of non-radiative lifetimes (τ_{32}/τ_{21}) at 77 K and 300 K for the range of three-level systems. It is clear that, for designs of this form, population inversion cannot be anticipated at room temperature. However, inversion is possible at 77 K, and it becomes stronger as the terahertz emission energy (emission frequency) is reduced, with a population ratio in excess of 5:1 predicted for
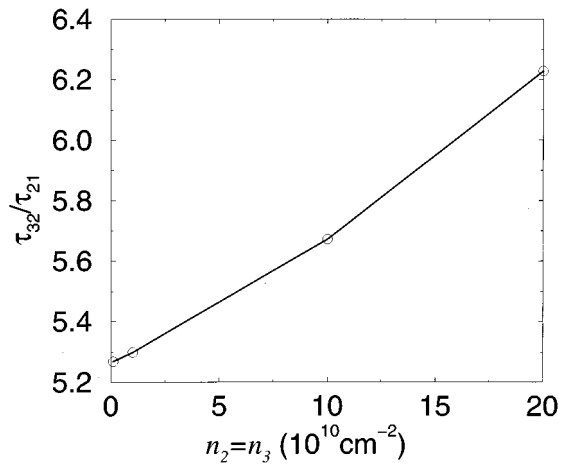
FIG. 5. Population dependence of the ratio of the non-radiative lifetime in the upper laser level to that in the lower level for the 2.8 THz three-level structure. $T = 77$ K.
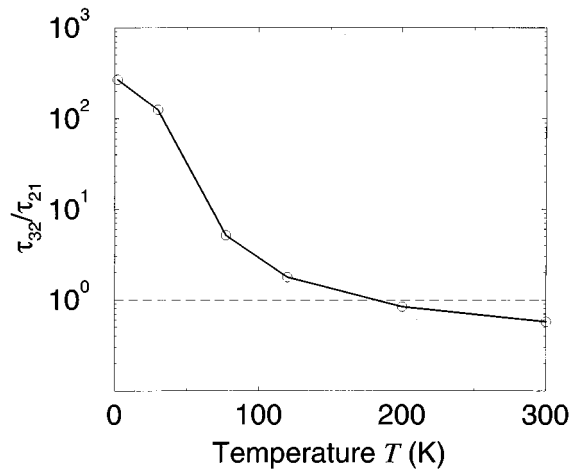

FIG. 6. Temperature dependence of the ratio of the non-radiative lifetime in the upper laser level to that in the lower level for the 2.8 THz three-level structure. $n_2 = n_3 = 10^{10}$ cm^{-2}.

the lowest frequency (2.8 THz) device. However, reducing the emission frequency will have a detrimental effect on the internal quantum efficiency, given by the ratio τ_{32}/τ_{rad}. Calculated values of τ_{rad} (for $T = 77$ K) are shown in Table I. These show a marked increase with decreasing emission energy. The quantum efficiency for a single active region is always going to be very poor (approx. 10^{-6}), but is over an order of magnitude smaller at 2.8 THz (the lowest emission frequency considered) than at 12.1 THz (the highest frequency considered). The lifetime ratios for $T = 2$ K are not shown in Fig. 3. These are predicted to be very high for all structures with $E_3 - E_2 < E_{LO}$; however it must be stressed that this prediction will be strongly affected by increases in electron temperature.

Figure 5 shows the effect of increasing pump intensity on the condition for population inversion for the most promising three-level system (the 2.8 THz emitter) at 77 K. The total carrier concentration in all three states is taken as 10^{12} cm^{-2} and, as before, for the sake of calculating the scattering rates the populations n_2 and n_3 are assumed equal (corresponding to marginal population inversion). A small increase in the population ratio is predicted with increasing pump power. The scattering rates show that this is almost entirely due to an increase in τ_{32}, due to band filling (Pauli exclusion effect) in the second subband.

The temperature dependence of the ratio of non-radiative lifetimes for the 2.8 THz emitter ($x_b = 18\%$ in Table I) is examined more closely in Fig. 6. Here lies the ultimate conclusion for an optically pumped three-level laser based on a single stepped quantum well and operating in the terahertz or far-infrared region of the spectrum. Figure 6 clearly shows that while strong population inversion may be possible at near-zero (e.g. liquid helium) temperatures (subject to the exact electron temperatures involved), it appears that stimulated emission, and hence laser operation, in such devices is not practical at room temperature. While a simple luminescent (spontaneous emission) device may be a possibility, a more sophisticated design will be necessary to acheive population inversion at room temperature, and it is for this reason

that the design is generalised to include an additional level with the aim of increasing the depopulation rate from the lower laser level.

B. Four-level system

The four-level system is again based on a single stepped quantum well. A typical structure is shown in Fig. 7. In this system, the $E_4 - E_1$ separation is maintained at the CO_2 pump energy, and terahertz emission is sought from transitions between subbands 4 and 3. The purpose of the additional level ($|2\rangle$) is to optimise de-population of the lower laser level ($|3\rangle$) by tuning the energy separation $E_3 - E_2$ to the LO phonon energy, thus enabling scattering by zero wave vector (q) phonons, for which the LO phonon scattering rate is maximised. To test this idea, a set of four-level structures were designed in which the barrier composition and deep well width were kept constant ($x = 24\%$ and $a = 140$ Å, respectively), while the step width (b) and height
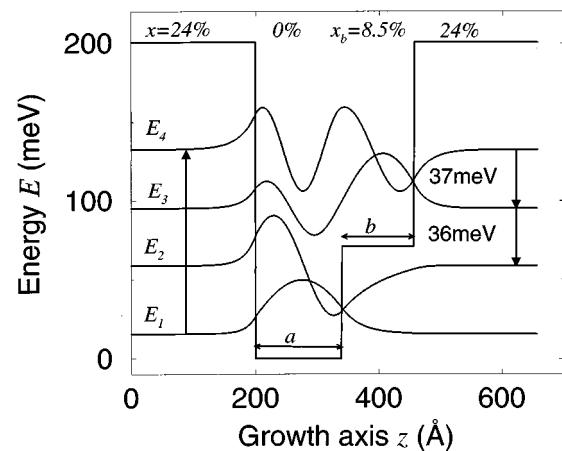

FIG. 7. Schematic diagram of the energy levels and wave functions of a four-level asymmetric quantum well. The system is designed for CO_2 pumping between levels 1 and 4 ($E_4 - E_1 = 117$ meV), and $E_3 - E_2$ is tuned to the LO phonon energy. The emission frequency for this particular device ($|3\rangle \rightarrow |2\rangle$ transitions) is 9.0 THz.

TABLE II. Structural parameters of a four-level asymmetric quantum well with a terahertz E_4-E_3 intersubband separation, with E_3-E_2 swept through the LO phonon energy.

Step x_b (%)	Step width b (Å)	E_4-E_1 (meV)	E_4-E_3 (meV)	E_4-E_3 (THz)	E_3-E_2 (meV)
6	102	116.811	45.872	11.1	32.396
7	107	116.939	42.838	10.4	33.435
8	113	117.112	39.379	9.5	35.297
8.5	117	117.002	37.414	9.0	36.372
9	121	117.069	35.420	8.6	37.728
10	131	117.079	31.139	7.5	40.769
11	145	116.880	26.478	6.4	44.234

TABLE III. Structural parameters of four-level systems satisfying the resonant depopulation criterion $E_3-E_2=E_{LO}$.

a (Å)	b (Å)	x_b (%)	E_4-E_3 (meV)	E_4-E_3 (THz)	E_3-E_2 (meV)	τ_{43}/τ_{32}
40	179	10	48.910	11.8	35.829	1.4590
80	149	6	44.366	10.7	35.375	1.1455
90	136	4	48.557	11.7	37.373	1.3297
100	700	17	2.628	0.6	36.734	0.0512
120	220	13	20.965	5.1	37.244	0.2957
130	163	11	29.612	7.2	36.722	0.4857
140	117	8.5	37.414	9.0	36.372	0.6994

(x_b) were varied as shown in Table II. This prescription yields a set of structures that have a range of terahertz emission frequencies, all with a fixed pump energy, while the E_3-E_2 separation is gradually swept through the LO phonon energy. However, the design constraints imposed on this system mean that the terahertz emission energy (E_4-E_3) cannot be maintained below E_{LO} for the whole range of structures in Table II.

Figure 8 shows the $|4\rangle\rightarrow|3\rangle$ and $|3\rangle\rightarrow|2\rangle$ non-radiative scattering rates at 300 K for the series of structures in Table II. Note that, for these four-level systems, the population inversion ratio is given (following the same analysis as above) by τ_{43}/τ_{32}. The $|4\rangle\rightarrow|3\rangle$ rate (which gives re-population of the lower laser level) has a maximum at $x_b=9\%$: at this point E_4-E_3 is closest to the LO phonon energy. As in the three-level system, the scattering rate is still substantial even when E_4-E_3 is less than E_{LO} (structures with $x_b>9\%$), indicating LO phonon emission by ''warm'' electrons in subband 4. The de-population rate for the lower laser level is given by $1/\tau_{32}$. This rate is substantially larger than the de-population rate for the three-level system (given by $1/\tau_{21}$ in Fig. 3), and is a direct consequence of the $1/q^2$ dependence of the Frölich matrix element for LO phonon scattering, which gives faster rates for near-vertical (small q) transitions. Thus, tuning the E_3-E_2 separation to

the LO phonon energy *is* an effective aid to de-population. However, there is no peak in the $|3\rangle\rightarrow|2\rangle$ scattering rate, even though E_3-E_2 is swept through the LO phonon energy. It transpires that, for these structures, it is the overlap between the $|3\rangle$ and $|2\rangle$ wave functions that is more important.

Figure 7 illustrates the zone centre wave functions of the first four subbands for the 9.0 THz emitter ($x_b=8.5\%$ in Table II). It can be seen that the lowest two states are localised within the GaAs well while the highest two states are above the energy step. However, as the step height is reduced (decreasing x_b), the second level shifts above the step. Both $|3\rangle$ and $|2\rangle$ wave functions are now localised across the same spatial region, and this leads to an increase in the scattering matrix element. The effect is sufficiently strong to predict room temperature population inversion in the $x_b=6\%$ device, even though E_3-E_2 is less than E_{LO}, and E_4-E_3 is greater than E_{LO}, both conditions contrary to the expected design ideals.

The effect of the wave function overlap is even more dramatically illustrated by another series of calculations (again at 300 K) in which the structures were designed such that the condition for resonant depopulation of subband 3 was always fulfilled. This was achieved by first choosing the deep well width a, and then adjusting the step height x_b and width b in order to satisfy both $E_4-E_1=117$ meV and $E_3-E_2=E_{LO}$. The structural parameters are listed in Table III. The emission energy and the ratio of non-radiative lifetimes are plotted in Fig. 9. Between $a=90$ Å and 100 Å there is a dramatic change in the electronic structure of the quantum wells: for $a\leqslant 90$ Å the system has three states confined in the GaAs deep well region, but for $a\geqslant 100$ Å there are only two. (This may seem counterintuitive given that a increases, but it must be remembered that the structures defined in Table III involve a complex variation of several structural parameters.) When E_3 shifts above the step potential, the E_4-E_3 separation collapses, as seen in Fig. 9 for $a=100$ Å. The population ratio mirrors the radiative transition energy. This is a reflection on the importance of the $1/\tau_{32}$ scattering rate which is critically dependent on the overlap between the wave functions. As state $|3\rangle$ moves above the step at $a=100$ Å, the overlap with state $|2\rangle$ is dramatically reduced, leading to a reduction in the de-population rate of the lower laser level and hence in the predicted population ratio.
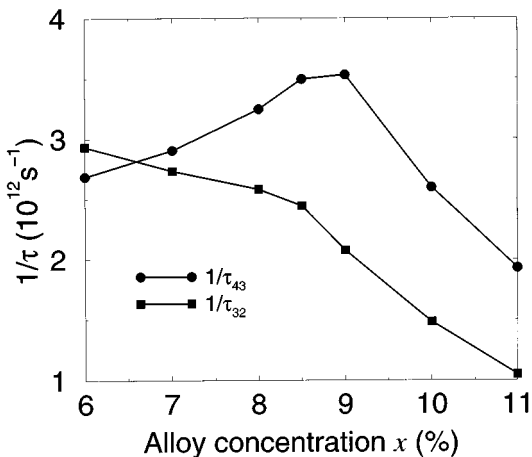

FIG. 8. The $|4\rangle\rightarrow|3\rangle$ and $|3\rangle\rightarrow|2\rangle$ non-radiative (phonon scattering) transition rates for the four-level asymmetric quantum wells, defined in Table II. $T=300$ K, $E_4-E_1=117$ meV throughout.
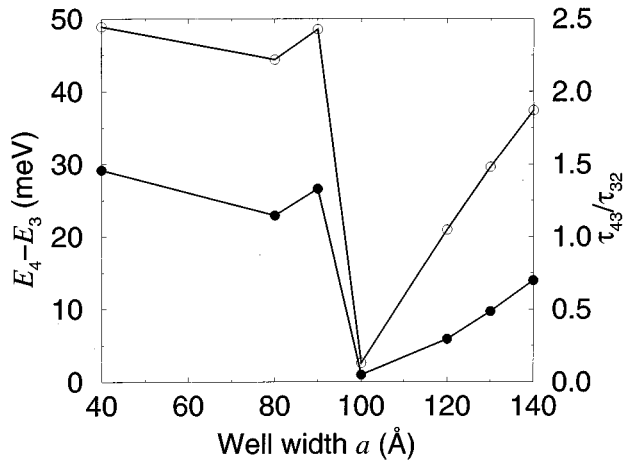
FIG. 9. Emission energy (hollow circles and left-hand axis) and the lasing condition (filled circles, right-hand axis) plotted against the well width a for a series of structures satisfying the resonant de-population condition $E_3 - E_2 = E_{LO}$, as in Table III. $T = 300$ K, $E_4 - E_1 = 117$ meV throughout.

The most interesting aspect of Fig. 9 is, of course, the fact that τ_{43}/τ_{32} is greater than unity for all structures defined by $a \leqslant 90$ Å in Table III. As with the previous set of four-level designs, room temperature population inversion is only predicted for structures in which $E_4 - E_3 > E_{LO}$, giving emission frequencies of approximately 10 THz. Thus, for the structures considered here, incomplete suppression of LO phonon scattering means that merely designing for a subband separation less than E_{LO} does not result in the highest population inversion ratio.

IV. CONCLUSIONS

Intersubband carrier lifetimes have been calculated for three- and four-level optically pumped asymmetric quantum wells designed for terahertz laser operation. It was shown that, in the three-level systems, the ratio of the carrier lifetimes in the upper and lower laser levels fulfills the necessary condition for stimulated emission only at cryogenic temperatures. Room temperature population inversion is precluded due to fast intersubband LO phonon scattering, which persists even in structures with subband separations less the the LO phonon energy, due to thermal broadening of the electron energy distribution.

Further calculations showed, however, that introducing a fourth level into the system, at exactly one LO phonon energy below the lower laser level, leads to an enhancement in the de-population rate and offers the potential for stimulated emission at room temperature.

[1] J. Faist, F. Capasso, C. Sitori, D. I. Sivco, A. L. Hutchinson, and A. Cho, Appl. Phys. Lett. **67**, 3057 (1995);

[2] D. Y. Oberli, D. R. Wake, M. V. Klein, J. Klem, T. Henderson, and H. Morkoç, Phys. Rev. Lett. **59**, 696 (1987).

[3] K. L. Schumacher, D. Collings, R. T. Phillips, D. A. Ritchie, G. Weber, J. N. Schulman, and K. Ploog, Semicond. Sci. Technol. **11**, 1173 (1996).

[4] Y. Lavon, A. Sa'ar, Z. Moussa, F. H. Julien, and R. Planel, Superlattices Microstruct. **19**, 1 (1996).

[5] F. H. Julien, A. Sa'ar, J. Wang, and J. P. Leburton, Electron. Lett. **31**, 838 (1995).

[6] F. H. Julien, Z. Moussa, P. Bouchard, Y. Lavon, A. Sa'ar, J. Wang, J.-P. Leburton, V. Berger, J. Nagle, and R. Planel, Superlattices Microstruct. **19**, 69 (1996).

[7] P. Harrison and R. W. Kelsall, Superlattices Microstruct. (to be published).

[8] P. Harrison, W. E. Hagston, and T. Stirner, Phys. Rev. B **47**, 16 404 (1993).

[9] M. Lundstrom, *Fundamentals of Carrier Transport* (Addison-Wesley, Reading, MA, 1990).

[10] T. Piorek, Ph.D. thesis, University of Hull, UK, 1996.

[11] M. Babiker, Semicond. Sci. Technol. **7**, B52 (1992).

[12] E. Molinari, C. Bungaro, M. Gulia, P. Lugli, and H. Rucker, Semicond. Sci. Technol. **7**, B67 (1992).

[13] B. K. Ridley, Phys. Rev. B **17**, 4592 (1993).

[14] B. K. Ridley, O. Al-Dossary, N. C. Constantinou, and M. Babiker, Phys. Rev. B **50**, 11 701 (1994).

[15] S. M. Goodnick and P. Lugli, Appl. Phys. Lett. **51**, 584 (1987).

[16] S. M. Goodnick and P. Lugli, Phys. Rev. B **37**, 2578 (1988).

[17] V. Berger, Semicond. Sci. Technol. **9**, 1493 (1994).

[18] M. Burt, J. Phys., Condens. Matter. **5**, 4091 (1993).

[19] D. T. F. Marple, J. Appl. Phys. **35**, 539 (1964).

[20] B. O. Seraphin and H. E. Bennett, in *Semiconductors and Semimetals*, edited by R. K. Willardson and A. C. Beer (Academic, New York, 1967), Vol. 3, p. 499.

[21] S.-C. Lee, I. Gallbraith, and C. R. Pidgeon, Phys. Rev. B **52**, 1874 (1995).

[22] B. N. Murdin, C. J. G. M. Langerak, M. Helm, P. Kruck, W. Heiss, V. Rosskopf, G. Strasser, E. Gornik, M. Dür, S. M. Goodnick, S.-C. Lee, I. Galbraith, and C. R. Pidgeon, Superlattices Microstruct. **19**, 17 (1996).